Quasiclassical Trajectory Study of the Atmospheric Reaction N(2 D) + NO(X 2 Π) → O(1 D) + N 2 (X 1 Σ g +)

ARTICLE *in* THE JOURNAL OF PHYSICAL CHEMISTRY A · JANUARY 2014

Impact Factor: 2.69 · DOI: 10.1021/jp408487y · Source: PubMed

3 AUTHORS:

Jing Li
University of Coimbra
14 PUBLICATIONS **44** CITATIONS
SEE PROFILE

Pedro J. S. B. Caridade
University of Coimbra
38 PUBLICATIONS **448** CITATIONS
SEE PROFILE

Antonio J. C. Varandas
University of Coimbra
382 PUBLICATIONS **6,749** CITATIONS
SEE PROFILE

THE JOURNAL OF PHYSICAL CHEMISTRY A

Article

pubs.acs.org/JPCA

Quasiclassical Trajectory Study of the Atmospheric Reaction N(^2D) + NO($X\ ^2\Pi$) → O(^1D) + N_2($X\ ^1\Sigma_g^+$)

Jing Li,[†] Pedro J. S. B. Caridade,[†] and António J. C. Varandas[†,‡,*]

[†]Departamento de Química, Universidade de Coimbra, 3004-535 Coimbra,Portugal

[‡]Centro de Química, Universidade de Coimbra, 3004-535 Coimbra, Portugal

ABSTRACT: Quasiclassical trajectories have been run for the title atmospheric reaction over the range of temperatures $5 \le T/\mathrm{K} \le 3000$ on a recently proposed single-sheeted double many-body expansion (DMBE) potential energy surface for ground-state $N_2O(^1A')$. As typical in a capture-like reaction, the rate constant decreases with temperature for $50 \le T/\mathrm{K} \le 800$ K, while showing a small dependence at higher temperature regimes. At room temperature, it is predicted to have a value of $(20.1 \pm 0.2) \times 10^{-12}$ cm^3 s^{-1}. The calculated cross sections show a monotonic decay with temperature and translational energy. Good agreement with the experimental data has been observed, providing more realistic rate constants and hence support of enhanced accuracy for the DMBE potential energy surface with respect to other available forms.

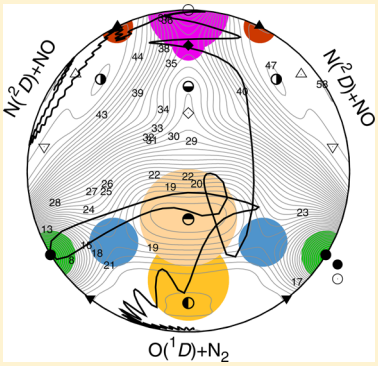

1. INTRODUCTION

Interest in the N_2O system has been increasing in recent years due to its key role in the ozone-depleting process.[1] In particular, the N(^2D,^4S) + NO reactions and dynamics have been the subject of much theoretical and experimental work due to their role in environmental issues.[2−9] Specifically, the reaction of N(^2D) with NO is a good prototype in collisional dynamics, as demonstrated by the many experimental measurements of the thermal rate constant for the total removal of N(^2D) by NO at 300 K.

There are several energetically accessible processes for the N(^2D) + NO collisional process at room temperature:

$$N_a(^2D) + N_bO(X^2\Pi) \rightarrow O(^3P) + N_2(X^1\Sigma_g^+) \quad \Delta E = -132.30\ \mathrm{kcal\ mol^{-1}} \tag{1}$$

$$\rightarrow O(^1D) + N_2(X^1\Sigma_g^+) \quad \Delta E = -86.87\ \mathrm{kcal\ mol^{-1}} \tag{2}$$

$$\rightarrow O(^1S) + N_2(X^1\Sigma_g^+) \quad \Delta E = -35.68\ \mathrm{kcal\ mol^{-1}} \tag{3}$$

$$\rightarrow N_a(^2D) + N_bO(X^2\Pi) \tag{4}$$

$$\rightarrow N_b(^2D) + N_aO(X^2\Pi) \tag{5}$$

where the subscripts a and b label the two nitrogen atoms. Processes 1−3 lead to formation of atomic oxygen in the fundamental or excited states, with the N_2 fragment left in its ground electronic state. Reactions 4 and 5 represent instead inelastic/elastic processes, and the exchange reaction of atomic nitrogen, respectively. Other important processes are those that involve the $^2D/^4S$ electronic quenching of the nitrogen atom (ΔE = 56.39 kcal mol^{-1}), but these are out of the scope of the present work.

The previous *ab initio* studies by Hopper[10] and Donovan and Husain[11] provided a detailed overview of the low-lying excited state potential energy surfaces (PESs) for the title system. From a total of 20 PESs [$5(^1A')$, $5(^1A'')$, $5(^3A')$, and $5(^3A'')$] which adiabatically correlate with reactants in C_s symmetry, there are $3(^1A')$ and $2(^1A'')$ PESs correlating with products for reaction 2, while only $^3A''$ and $^1A'$ PESs are associated with reactions 1 and 3, respectively. Furthermore, the existence of five adiabatic PESs involved in reaction 2 suggests that this exothermic process should significantly contribute to the N(^2D) total removal rate constant.

Reaction 2 is important in both atmospheric and combustion processes because it is a source of highly reactive oxygen atoms in the first excited state.[12] However, only a few experimental kinetic studies are available dealing with the thermal rate constant for the total removal of N(^2D) by NO at 300 K. The earlier determination by Black et al.[13] analyzed the transient measurements of NO (β) emission to give the rate coefficients for removal of N(^2D) by several simple molecules, which predicted a rate constant of $(180 \pm 50) \times 10^{-12}$ cm^3 s^{-1}. In 1971, the line absorption technique was applied by Lin and Kaufman[14] to the kinetic study of the metastable atomic nitrogen N(^2D) in a flowing afterglow system. Their measurements led to a rate constant at room temperature of $(70 \pm 25) \times 10^{-12}$ cm^3 s^{-1}. Husain et al. obtained values of[15] $(61 \pm 37) \times 10^{-12}$ cm^3 s^{-1} and[16] $(59 \pm 4) \times 10^{-12}$ cm^3 s^{-1} using a fast flow technique. In turn, the lowest value of $(35 \pm 3) \times 10^{-12}$ cm^3 s^{-1}

Received: August 24, 2013
Revised: January 28, 2014
Published: January 30, 2014

   dx.doi.org/10.1021/jp408487y | J. Phys. Chem. A 2014, 118, 1277−1286

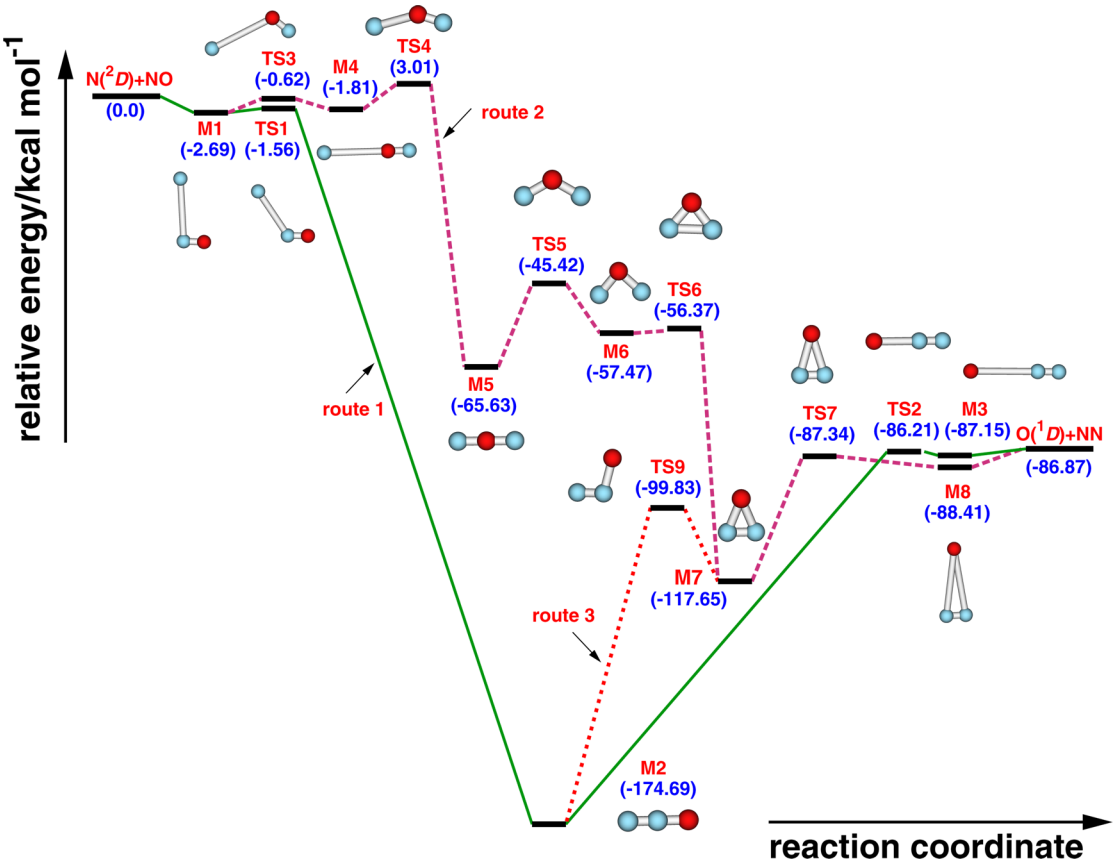

Figure 1. Energy diagram of the stationary points located on the DMBE PES. Energies are given relative to the N(^2D) + NO asymptote (in kcal mol^{-1}). The existence of several reaction pathways through which the system can evolve along the $^1A'$ PES has been shown in terms of the labeled routes 1 (drawn in green solid line), 2 (indicated in dark-pink dashed line), and 3 (links routes 1 and 2, shown in red dotted line).

reported by Sugawara et al.[17] using the pulse-radiolysis technique for measurement of the quenching rates of the metastable nitrogen atom, ^2D and ^3P in both nitrogen and helium, has been attributed to a flaw in their method of obtaining the NO partial pressure. Not surprisingly, therefore, the recommended room temperature rate constant, 60×10^{-12} cm^3 s^{-1}, is based on the data of Lin and Kaufman,[14] Husain et al.,[15,16] and Umemoto et al.[18] Although there is no certainty on the formed product states in such studies,[11] the reaction most likely leads to formation of $N_2(X\ ^1\Sigma_g^+)$ + O(^3P,^1D,^1S), which thence forms atomic oxygen in all allowed electronic states.

The N_2O system for the first singlet $^1A'$ has been extensively studied both experimental and theoretically. However, for the PES of the N_2O molecule, the majority of structural studies focused on its global minimum, with this information being also of relevance for the reaction of concern. Theoretical studies of nitrous oxide date back to the first two-dimensional PESs calculated by Brown et al.[19] with the NN bond length kept fixed at the experimental value of 1.1282 Å, which predicted a well depth of −80.41 kcal mol^{-1} relative to O(^1D) + $N_2(X\ ^1\Sigma_g^+)$, thence within 8% of the experimental dissociation energy of −87.25 kcal mol^{-1} and which has been subsequently used by Johnson et al.[20] in dynamics calculations. Improved electronic structure calculations have been performed later by Daud et al.[21] using the complete-active-space self-consistent field (CASSCF) and the multireference configuration interaction (MRCI) electronic structure methods, still keeping the NN bond fixed at the equilibrium value. At the same time, Nanbu and Johnson[22] reported full three-dimensional PESs and employed them in dynamics calculations. Schinke[23] calculated the ground state PESs, which show a minimum of −85.63 kcal mol^{-1} for a linear NNO structure, and used them for wave packet dynamics.[24−26] However, theoretical studies of the N(^2D) + NO($X\ ^2\Pi$) reactions are very scarce, with González et al.[27] being the only authors to make an extensive theoretical study of the N(^2D) + NO($X\ ^2\Pi$) → O(^1D) + $N_2(X\ ^1\Sigma_g^+)$ exothermic reaction. The resulting PES (heretofore denoted GRR PES) has been employed for quasi-classical trajectory (QCT) calculations, and obtained a value of $(2.63 \pm 0.07) \times 10^{-12}$ cm^3 s^{-1} at room temperature, thus largely underestimating the total experimental rate constant.

The present study has a dual purpose: first, to test the accuracy of our recently proposed double many-body expansion[28−30] (DMBE) PES for the title system[31] based on MRCI(Q)[32,33] (multireference configuration interaction including the Davidson correction) energies, using the aug-cc-pVTZ (AVTZ) basis set of Dunning;[34,35] second, to improve our understanding of the results for the rate constant and cross sections within the QCT dynamical approach here employed. State-specific QCT cross sections and thermalized rate constants have therefore been calculated using the newly reported N_2O ($^1A'$) DMBE PES.[31] The paper is structured as follows. Section 2 gives a brief survey of the PES and utilized computational methods, while the results and discussion are in section 3. The concluding remarks are summarized in section 4.

dx.doi.org/10.1021/jp408487y | J. Phys. Chem. A 2014, 118, 1277−1286

2. CALCULATION DETAILS

2.1. Potential Energy Surface. Dynamics calculations have been performed previously on a many-body expansion[36] (MBE) PES constructed by González et al.[27] for the ground state ($^1A'$) of N_2O. They performed CASSCF electronic structure calculations, followed by second-order perturbation theory calculations using the CASSCF wave function as reference (CASPT2). Both studies employed the standard Cartesian 6-311G(2d) basis set of Pople and co-workers,[37,38] predicting a well depth of −170.9 kcal mol^{-1} relative to the N(^2D) + NO($X\ ^2\Pi$) dissociation limit.

In this work we have employed the global single-sheeted DMBE PES that we have recently reported based on a least-squares fit to a set of high level MRCI(Q)/AVTZ *ab initio* energies, which have been suitably corrected using the DMBE-scaled external correlation[39] (DMBE-SEC) method. A total of 809 points covering a range of energy up to ∼500 kcal mol^{-1} above the N_2O global minimum have been used for the calibration procedure, with the total rmsd being 0.940 kcal mol^{-1}. One of the most important properties of the DMBE PES is the proper description of the long-range forces, which, in this case, are of major relevance for the N(^2D) + NO reaction. Since this DMBE PES has been described in detail elsewhere, the reader is directed elsewhere[31] for a more detailed description.

The global minimum of ground-state N_2O has a linear (N−N−O) geometry, which in the DMBE PES here utilized is predicted to be located at R_{NN} = 1.1399 Å, and R_{NO} = 1.1928 Å, with a well depth of −174.69 kcal mol^{-1} and −89.63 kcal mol^{-1} relative to the N(^2D) + NO($X\ ^2\Pi$) and O(^1D) + N_2($X\ ^1\Sigma_g^+$) dissociation channels, respectively. The energy differences with respect to the experimental data are of 2.19 kcal mol^{-1} and 2.38 kcal mol^{-1}, with relative errors smaller than 1.2% and 2.7% (respectively), thence in very good accordance with the experimental data. Figure 1 displays the minima and transition states predicted on the DMBE PES and their relative energies. From this plot, several reactive paths can be distinguished in terms of the routes labeled 1, 2, and 3, with the most likely minimum energy path for the title reaction being via N(^2D) atom attack to the N end of the NO molecule (M1), through the transition state TS1, then evolving through the global minimum (M2), the linear barrier (TS2), and the minimum M3, and finally dissociating to products (route 1).

Figure 2 shows a relaxed triangular plot[40] utilizing the reduced hyperspherical coordinates $\beta^* = \beta/Q$ and $\gamma^* = \gamma/Q$:

$$\begin{pmatrix} Q \\ \beta \\ \gamma \end{pmatrix} = \begin{pmatrix} 1 & 1 & 1 \\ 0 & \sqrt{3} & -\sqrt{3} \\ 2 & -1 & -1 \end{pmatrix} \begin{pmatrix} R_1^2 \\ R_2^2 \\ R_3^2 \end{pmatrix} \tag{6}$$

Besides illustrating in a single plot all important topographical features of the PES, such a plot can also be used to visualize the trajectories run.[41] An example of a short-lived reactive trajectory is actually shown there by the wigly line. The colored circles indicate regions utilized for the assignment of reactive trajectories to passage over specific stationary points.

2.2. Quasiclassical Trajectory Calculations. All dynamics calculations here reported have utilized the QCT method, which is widely described in the literature.[42] The classical equations of motion have been integrated using a time step of 0.2 fs, such as to warrant conservation of the total energy within

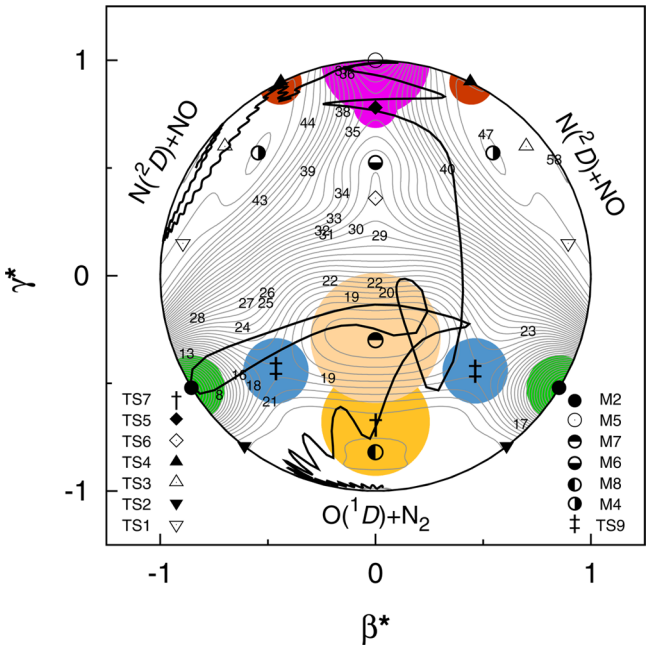

Figure 2. Relaxed triangular plot in hyperspherical coordinates illustrating the location and symmetry of all stationary points located on the DMBE PES. The circles in different colors refer to the estimation of the reactive trajectories passing the certain stationary point. Juxtaposed on this plot as the solid line is a short-lived reactive trajectory.

0.01 kcal mol^{-1} or smaller, with the reactants initially separated by 19 Å. All remaining dynamical parameters have been obtained by the standard QCT procedure. The reactive cross section for the state-specific (v = 0, j = 1) can be calculated using the traditional expression

$$\sigma_r(E_{tr};\ v = 0, j = 1) = \pi b_{max}^2 \frac{N_r}{N} \tag{7}$$

with the 68% statistical uncertainty being given by $\Delta\sigma_r = \sigma_r[(N - N_r)/(NN_r)]^{1/2}$. The symbols have their usual meaning: N_r is the total number of reactive trajectories out of a set of N integrated ones, and b_{max} is the maximum impact parameter for the reaction, which has been determined in the traditional way.[42] The state-specific rate constant is then given by averaging the cross section over the translation energy

$$k_{vj}(T) = g_e(T)\left(\frac{8k_BT}{\pi\mu_{N+NO}}\right)^{1/2}\left(\frac{1}{k_BT}\right)^2 \int_0^\infty E_{tr}\sigma_r \times \exp\left(-\frac{E_{tr}}{k_BT}\right) dE_{tr} \tag{8}$$

where μ_{N+NO} is the reduced mass of the reactants, and k_B the Boltzmann constant. Because the dynamics is performed adiabatically on the $^1A''$ state, the electronic degeneracy factor assumes the form

$$g_e(T) = q_{N_2O}(T)\ q_{N(^2D)}^{-1}(T)\ q_{NO(^2\Pi)}^{-1}(T) \tag{9}$$

with the electronic partition functions accounting for the fine-structure of N(^2D) and NO($^2\Pi$):

$$q_{N_2O} = 1 \tag{10}$$

dx.doi.org/10.1021/jp408487y | J. Phys. Chem. A 2014, 118, 1277−1286

$$q_{N(^2D)}(T) = 6 + 4\exp(-12.53/T) \quad (11)$$

$$q_{NO(^2\Pi)}(T) = 2 + 2\exp(-177.1/T) \quad (12)$$

The thermal rate constant can be obtained by averaging the internal states of the NO molecule and translational energy:

$$k(T) = g_e(T)\left(\frac{2}{k_BT}\right)^{3/2}\left(\frac{1}{\pi}\right)^{1/2} Q_{vj}^{-1}(T)\sum_{vj}(2j+1) \times \exp\left(-\frac{E_{vj}}{k_BT}\right)\int_0^\infty E_{tr}\sigma^x \exp\left(-\frac{E_{tr}}{k_BT}\right) dE_{tr} \quad (13)$$

where $Q_{vj}(T)$ the rovibrational partition function and E_{vj} the (v,j) state energy. The cumulative function of the translation energy sampling assumes the form.[42,43] $E_{tr} = k_BT\ln(\xi_1\xi_2)$, where ξ_i are freshly generated random numbers (see elsewhere[44] for an alternative scheme).

For a realistic sampling of the internal states of the NO diatomic, the method described in ref 45 has been adopted. It starts with the cumulative rovibrational Boltzmann distribution

$$C(v,j;T) = \sum_{v'=0}\sum_{j'=1}(2j'+1)\exp(-E_{v'j'}/k_BT)Q_{v'j'}^{-1}(T) \quad (14)$$

where $Q_{vj}(T)$ is the rovibrational partition function for all the states of NO($X\ ^2\Pi$), with the rovibrational energies calculated by solving the nuclear Schrödinger equation for the diatomic fragment.[46] Note that the sum in eq 14 is over rovibrational states, thus avoiding the traditional energy partitioning into vibrational and rotational components. For each temperature, the (v, j) state is sampled via eq 14 when the condition $C(v,j;T) \geq \xi_3$ is satisfied for a freshly generated random number, ξ_3.

For vibrational state-specific calculations, eq 14 is also used by summing only the rotational states for a fixed v, and $Q_{vj}^{-1}(T)$ is the rotational partition function for that specific vibrational state. The thermal rate constant is then obtained as

$$k(T) = g_e\left(\frac{8k_BT}{\pi\mu_{N+NO}}\right)^{1/2}\pi b_{max}^2\frac{N_r}{N} \quad (15)$$

with the corresponding error being given by $\Delta k(T) = k(T)[(N - N_r)/(NN_r)]^{1/2}$. A total of 10^5 trajectories have been run for T = 300 K, and 10^4 for the other temperatures, which were considered sufficient to obtain a low statistical deviation for all the studied properties.

3. RESULTS AND DISCUSSION

3.1. Rate Constants. As pointed out in the Introduction, experimental information on the studied reaction is scarce, referring only to the total N(^2D) + NO($X\ ^2\Pi$) rate constant at room temperature (around 300 K). Thus, a direct comparison between the calculated and experimental rate constants is not free of some ambiguity. Table 1 compares the calculated rate constants at room temperature with the total removal of N(^2D) by NO and the calculated QCT result. To a first approximation on accounting for the total reactivity of the system, the ground-state $^1A'$ will yield a value of $k(300) = (20.1 \pm 0.2) \times 10^{-12}$ cm^3 s^{-1} at room temperature. Such a result yields only about one-third of the experimental rate constant, $k = 60 \times 10^{-12}$ cm^3 s^{-1} for the total reaction in N(^2D) + NO($X\ ^2\Pi$).

Table 1. Rate Constants for the N(^2D) + NO($X\ ^2\Pi$) at Room Temperature ($T \approx 300$ K)

source	year	method	$k/10^{-12}$ cm^3 s^{-1}
Black et al.[13]	1969	FP-CL	180 ± 50
Lin and Kaufman[14]	1971	DF-RA	70 ± 25
Husain et al.[15]	1972	FP-RA	61 ± 37
Husain et al.[16]	1974	FP-RA	59 ± 4.0
Sugawara et al.[17]	1980	PR-RA	35 ± 3.0
Fell et al.[47]	1990	LP-LIF	67 ± 13
Umemoto et al.[18]	1998	LP-LIF	82.7 ± 2.9
González et al.[27]	2000	QCT	2.63 ± 0.07
this work	2012	QCT	20.3 ± 0.1

As stated in the Introduction, the total experimental rate constant is a sum of the rate constants of every process that can be responsible for the depletion of N(^2D), with the reaction almost certainly forming $N_2 + O(^3P,^1D,^1S)$. Indeed, there are 1 ($2^3A''$), 5[$1^1A'$, $2^1A'$, $3^1A'$, $1^1A''$, and 2 $^1A''$] and 1 ($4\ ^2A'$) PESs that correlate with products for reactions 1, 2, and 3, respectively. González et al.[27] have tried to take into account the reactivity due to the other four excited PESs connecting with products. They calculated the energies of these states with an equally weighted state-average over the states considered in selected points of an approximation barrier in the entrance NNO channel using the CASPT2 method, and they reported that at least the two first 1 $^1A'$ PESs, whose barriers are below 1 kcal mol^{-1}, would contribute significantly to reactivity at a temperature of 300 K. Briefly, they concluded that the rate constant for reaction 2 could reasonably be within the range 2.6 × 10^{-12} cm^3 s^{-1} with $1^1A'$ contribution to 7.9 × 10^{-12} cm^3 s^{-1}, if a similar contribution of the $1^1A'$, $2^1A'$ PESs to the total rate constant were assumed. In particular, the ground state $1^1A'$ with a deep well which is barrierless for the linear abstraction mechanism in reaction 2 suggests that this exothermic reaction should furnish an important contribution to the N(^2D) total removal rate constant. Clearly, our result is reasonable and substantially larger (about 8 times) than the QCT result obtained from the MBE PES.[27] Such a difference may be explained due to the fact that the DMBE potential energy surface is based on a set of MRCI(Q)/AVTZ *ab initio* energies, which have been suitably corrected using the DMBE-scaled external correlation (DMBE-SEC) method. It shows a well depth of −174.69 kcal mol^{-1} and −89.63 kcal mol^{-1} relative to the N(^2D) + NO($X\ ^2\Pi$) and O(^1D) + $N_2(X\ ^1\Sigma_g^+)$ dissociation channels, respectively, which amount to energy differences more attractive than the experimental values by only 2.19 kcal mol^{-1} and 2.38 kcal mol^{-1}. Note that the PES of ref 27 is based on second-order perturbation theory calculations using the CASSCF wave function as reference (CASPT2) with the standard Cartesian 6-311G(2d) basis set: it has a well depth of −170.9 kcal mol^{-1}, with the N(^2D) + NO($X\ ^2\Pi$) dissociation limit lying higher than the experimental value by 1.6 kcal mol^{-1}. Another important feature of the DMBE PES concerns the proper description of long-range forces which are critical for a quantitative description of the title reaction.

Table 3 summarizes the thermally averaged rate constants for the N(^2D) + NO($X\ ^2\Pi$) reaction. The calculations cover the range of temperatures from 5 to 3000 K, with a total of 10 000 trajectories being integrated for each temperature. Figure 3 compares the calculated rate constants vs temperature with the experimental and previous QCT results. As inferred from Figure 3, the results of the title reaction can be divided into two

dx.doi.org/10.1021/jp408487y | J. Phys. Chem. A 2014, 118, 1277−1286

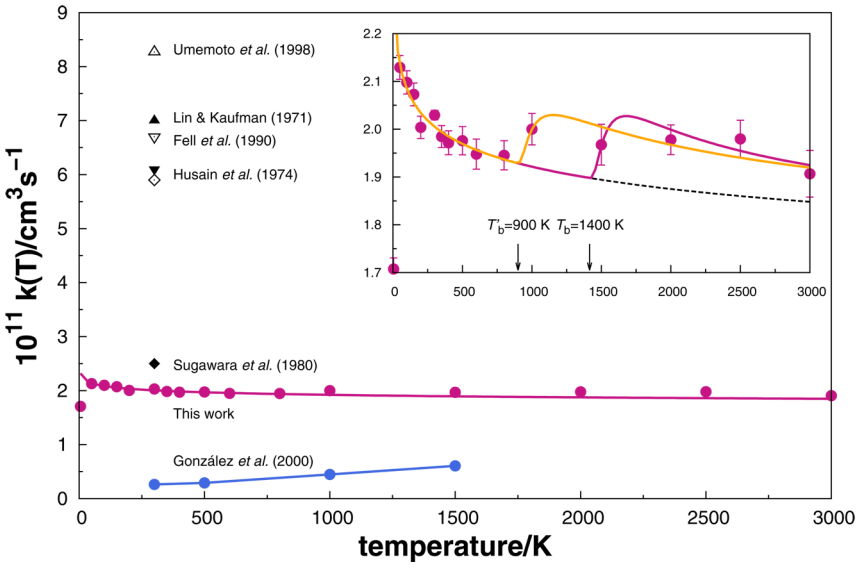

Figure 3. Rate constant for the $N(^2D) + NO(X\,^2\Pi) \rightarrow O(^1D) + N_2(X\,^1\Sigma_g^+)$ reaction as a function of temperature. The open circle symbols refer to the QCT calculations, while the solid curves through the data correspond to the best least-squares fits of eq 12. The fits are shown as a blue solid line and a red dashed line with T_b fixed at 900 and 1400 K, and the black dotted line corresponds to the fit of capture type eq 13 (see inset). Also shown are results reported by González et al. and the experimental values for the total removal of $N(^2D)$ by NO.

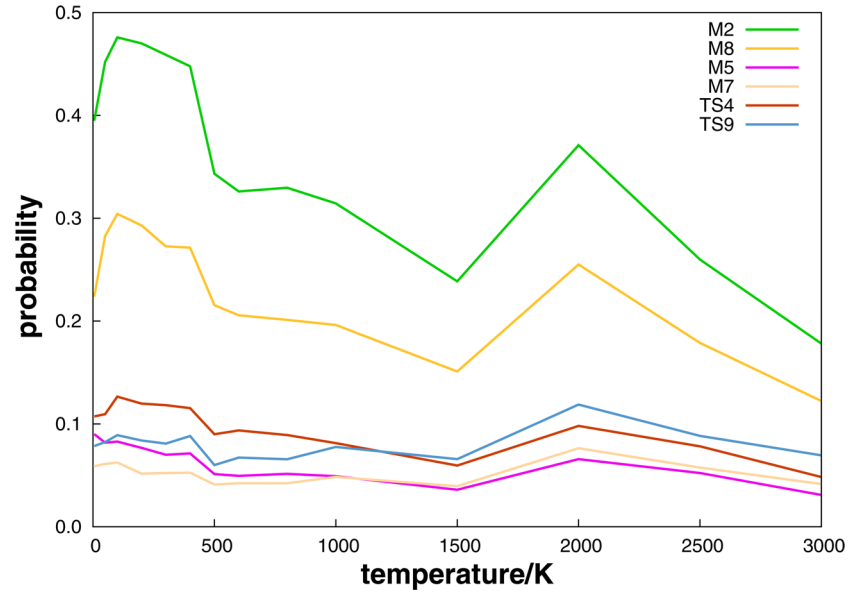

Figure 4. Reaction probability that may be approximately ascribed to various stationary points as a function of temperature.

parts. At low temperatures (from 50 to 800 K) the rate constant of reaction 2 decreases with T, as is typical of a capture-like reaction, while at 1000 K it increases and then decreases again until 3000 K although showing only a small dependence on the temperature. To model the calculated rate constants, we have therefore employed the composite form,

$$k(T) = k_{cap}(T) + k_b(T) \tag{16}$$

where k_{cap} accounts for the rate constants due to capture of a nitrogen atom from NO and k_b is a rate constant that is operative at high temperatures after overcoming the barrier in the entrance channel. As an aid to classify the different types of rate constants, we have employed the forms[48]

$$k_{cap}(T) = g_e(T)\left[\frac{2^{(3n-4)/2n} n\pi^{1/2}}{(n-2)^{(n-2)/n}\mu^{1/2}} \times \Gamma\left(\frac{2n-2}{n}\right)(k_B T)^{(n-4)/2n} C_n^{2/n}\right] \quad (T < T_b) \tag{17}$$

$$k_b(T) = g_e(T) A (T - T_b)^m \exp[-B/(T - T_b)] \quad (T \geq T_b) \tag{18}$$

leading to optimum least-squares parameters of n = 3.74, C_n = 1.69 $E_h a_0^n$, and $A = 6.41 \times 10^{-9}$ K^{-m} cm^3 s^{-1}, B = 221.11 K, m = −0.7093 for T_b fixed at 1400 K, while $A' = 1.35 \times 10^{-9}$ K^{-m} cm^3 s^{-1}, B' = 117.31, m' = −0.4959 for T_b fixed at 900 K.

As Figure 3 shows, the above fit mimics the calculated rate constant over the entire range of temperatures considered in

dx.doi.org/10.1021/jp408487y | J. Phys. Chem. A 2014, 118, 1277−1286

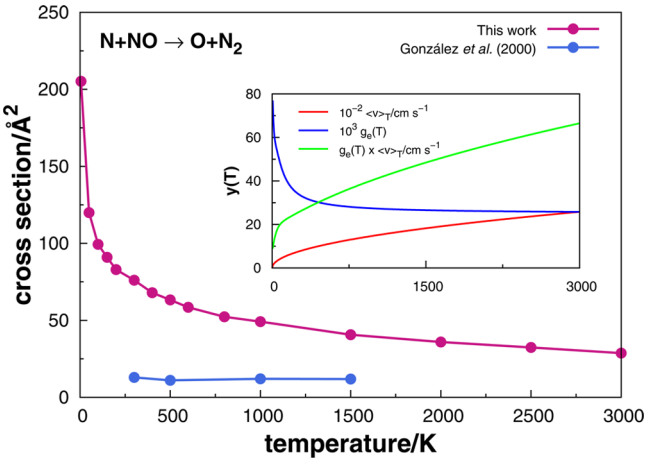

Figure 5. Cross section (Å^2) for the reaction N(^2D) + NO($X\ ^2\Pi$) → O(^1D) + N$_2$($X\ ^1\Sigma_g^+$) as a function of temperature. Also shown are $g_\epsilon(T)$ with the same form in eq 15, $\langle v\rangle_T = (8k_BT/\pi\mu_{N+NO})^{1/2}$, and $g_\epsilon(T)\langle v\rangle_T$.

Table 2. QCT Cross Sections for N(^2D) + NO($X\ ^2\Pi$) Reaction as a Function of Collision Energy

	N$_2$ + O				N-exchange		
E_{tr}/eV	b_{max}/Å	$100P_r$	σ_r/Å^2	$100\Delta\sigma_r$/Å^2	$100P_r$	σ_r/Å^2	$100\Delta\sigma_r$/Å^2
0.1	7.1	79.9	126.5	89.8	4.8	7.5	47.7
0.3	6.5	75.6	100.3	80.6	4.8	6.4	40.1
0.5	6.2	73.5	88.8	75.3	2.7	3.3	27.8
1.0	5.8	67.7	71.5	69.9	2.3	2.5	22.5
1.5	5.6	63.2	62.3	67.2	2.8	2.7	22.9
2.0	5.4	61.8	56.6	63.0	3.0	2.7	22.0
3.0	5.2	57.7	49.0	59.3	3.2	2.7	21.2
4.0	5.0	56.9	44.7	55.0	2.8	2.2	18.4
5.0	4.8	56.4	40.8	50.8	3.3	2.4	18.3
7.0	4.6	54.5	36.2	46.8	2.9	2.0	15.9
8.0	4.5	54.4	34.6	44.8	2.7	1.7	14.6
10.0	4.3	54.4	31.6	40.9	3.0	1.7	14.6

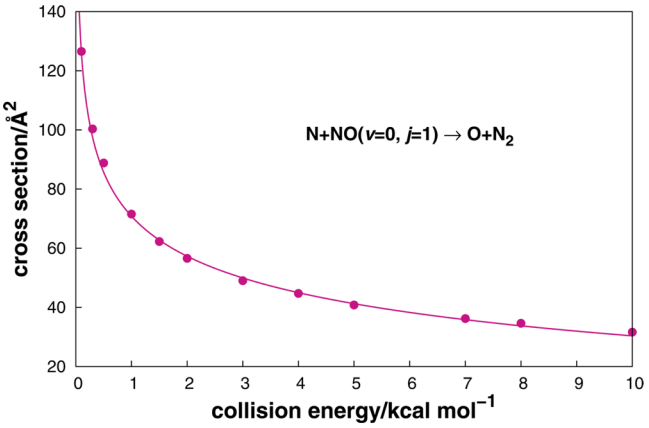

Figure 6. Estimated state-specific cross section (Å^2) for the reaction N(^2D) + NO(v = 0,j = 1) as a function of the collision energy.

the present work, with the threshold temperature fixed at T_b = 1400 K and T_b' = 900 K. Within the T range between 50 and 800 K, the rate constant changes from (21.3 ± 0.3) to (19.5 ± 0.3) × 10^{-12} cm^3 s^{-1}. The analysis for reaction at low temperature ($T < T_b$, T_b') indicates that most of the trajectories only traverse TS1, heading for the NNO minimum and dissociating to the products (see Figure 1 of route 1). At higher temperatures, the rate constant increases to (20.0 ± 0.3) × 10^{-12} cm^3 s^{-1} at 1000 K and then decreases to (19.1 ± 0.5) × 10^{-12} cm^3 s^{-1} at the highest temperature considered: T = 3000 K. There is a significant enhancement of the other reaction pathways: despite the magnitude of the entrance barriers, the N(^2D) atom could attack the NO oxygen side, leading to products through the reaction pathway route 2 (shown in Figure 1). Note that in fit I the threshold temperature has been fixed at 900 K, corresponding to a barrier value of 1.79 kcal mol^{-1} excluding the zero-point energy (ZPE) correction, and mimics all points. A fit II has been carried out where the T_b was fixed at 1400 K, passes through a maximum as the temperature increases, and then decreases at a rate determined by the parameter m, while the point at 1000 K was omitted in this fit procedure. Moreover, at the lowest temperature explored, the rate constant goes down to (17.1 ± 0.2) × 10^{-12} cm^3 s^{-1}. This may be attributed to the following mechanistic interpretation: although the magnitude of the entrance barrier facilitates an attack of the N(^2D) atom to the nitrogen side of its counterpart NO, traversing TS1 with a barrier of −1.56 kcal mol^{-1} and heading for the global minimum, in some trajectories the N(^2D) atom could attack the oxygen side of NO, proceeding to reaction pathway route 2, then returning to TS1, evolving through the global minimum to the products at a very low temperature. Also shown in Figure 3 are the experimental and theoretical data from the literature. As noted above, our results are more realistic and much larger than the QCT values obtained by González et al.[27] but, unlike the latter, show a near invariance with temperature in the covered range.

We have tried to account for the probabilities of the reactive trajectories passing via specific stationary points (or regions associated with them, as indicated by the colored circles in Figure 2), with the results being shown in Figure 4. As noted above, the calculated probabilities are in accordance with the rate constant as a function of temperature. The calculated probabilities show a decrease with increasing temperature at temperatures less than T_b, present a small peak at T = 2000 K, and attain the largest value when passing through the global minimum M2. This may be explained by noting that most reactive trajectories follow route 1 by forming a collision complex close to collinear NNO structures at low temperatures, while at high temperatures the trajectories can overcome the barrier and eventually evolve through less attractive regions of the PES, such as the ones involving bent NNO structures. Note also that the reaction probability involving TS4 and M4 is also significant. Indeed, N(^2D) may evolve through route 2, and even interchange routes.

3.2. Cross Sections. The calculated thermal cross sections for reaction 2 are reported in Table 3 and represented in Figure 5. For a given temperature and using the rovibrational and translational energy samplings of the previous section, a thermal cross section may be defined as $\sigma(T) = \pi b_{max}^2 N_r/N$, in which N_r is the number of reactives out of a batch of N trajectories. As seen, the reaction cross section decreases with T from 5 to 3000 K, with a sharp decrease from (205 ± 3) Å at 5 K to (120 ± 1) Å^2 at 50 K. More generally, it decreases monotonically over a wide range of temperature (T = 100−3000 K), namely from (99 ± 1) to (28.7 ± 0.7) Å^2. We analyzed various contributions of eq 15 (see the inset), with the term $\langle v\rangle_T = (8k_BT/\pi\mu_{N+NO})^{1/2}$, making a major contribution to such an unusual behavior in such a manner that the largest cross section turns out to yield the lowest rate constant at 5 K;

dx.doi.org/10.1021/jp408487y | J. Phys. Chem. A 2014, 118, 1277−1286

Table 3. Summary of the QCT Results for the $N(^2D)$ + $NO(X\ ^2\Pi)$ Reaction[a]

	N_2 + O			N-exchange			
T/K	b_{max}/Å	N_r[b]	σ_r/Å^2	$10^{12}k(T)$/ cm^3 s^{-1}	N_r[b]	σ_r/Å^2	$10^{13}k(T)$/ cm^3 s^{-1}
5	13.6	3531	205 ± 3	17.1 ± 0.2	231	13.4 ± 0.9	11.2 ± 0.7
50	9.5	4230	120 ± 1	21.3 ± 0.3	220	6.2 ± 0.4	11.1 ± 0.7
100	8.6	4276	99 ± 1	20.9 ± 0.3	192	4.5 ± 0.3	9.4 ± 0.7
150	8.2	4305	91 ± 1	20.7 ± 0.3	152	3.2 ± 0.3	7.3 ± 0.6
200	7.9	4230	83 ± 1	19.9 ± 0.3	123	2.4 ± 0.2	5.8 ± 0.2
300	9.2	28612	76.1 ± 0.4	20.3 ± 0.1	752	2.0 ± 0.1	5.3 ± 0.2
300[c]	6.0		12.9 ± 0.2	2.63 ± 0.04		0.023 ± 0.011	
400	7.5	3843	67.9 ± 0.9	19.7 ± 0.3	117	2.1 ± 0.2	6.0 ± 0.6
500	8.1	3068	63 ± 1	19.8 ± 0.3	72	1.5 ± 0.2	4.6 ± 0.5
500[c]	5.13		11.07 ± 0.3	2.92 ± 0.08		0.010 ± 0.005	
600	8.2	2766	58.4 ± 0.9	19.5 ± 0.3	60	1.3 ± 0.2	4.2 ± 0.5
800	7.6	2882	52.3 ± 0.8	19.5 ± 0.3	88	1.6 ± 0.2	5.9 ± 0.6
1000	7.6	2707	49.1 ± 0.8	20.0 ± 0.3	71	1.3 ± 0.2	5.3 ± 0.6
1000[c]	4.59		12.03 ± 0.28	4.48 ± 0.11		0.25 ± 0.04	
1500	8.6	1748	40.6 ± 0.9	19.7 ± 0.4	62	1.4 ± 0.2	7.0 ± 0.9
1500[c]	4.47		11.89 ± 0.29	6.06 ± 0.12		0.37 ± 0.04	
2000	6.3	2878	35.9 ± 0.6	19.8 ± 0.3	159	2.0 ± 0.2	10.9 ± 0.9
2500	7.1	2047	32.4 ± 0.6	19.8 ± 0.4	140	2.2 ± 0.2	14 ± 1
3000	8.3	1325	28.7 ± 0.7	19.1 ± 0.5	110	2.4 ± 0.2	16 ± 1

[a]Reaction channel: $N_a(^2D)$ + $N_bO(X\ ^2\Pi)$ → $O(^1D)$ + $N_2(X\ ^1\Sigma_g^+)$ (2) and $N_a(^2D)$ + $N_bO(X\ ^2\Pi)$ → $N_b(^2D)$ + $N_aO(X\ ^2\Pi)$. [b]100 000 trajectories calculated at 300 K and 10 000 otherwise. [c]QCT results from ref 27.

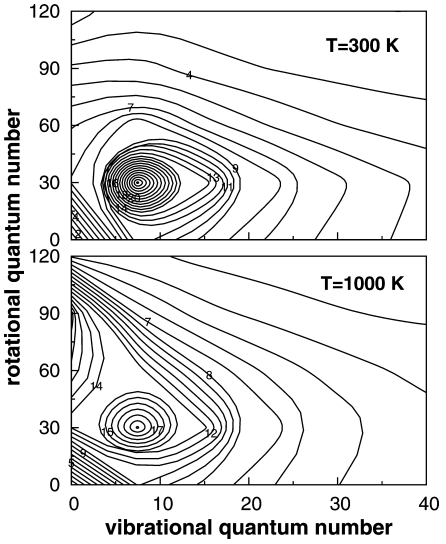

Figure 7. Comparison of the rovibrational distribution of the products of the title reaction on DMBE PESs for T = 300 and 1000 K. The lines are the probability contours starting at 0 and space by 0.00002.

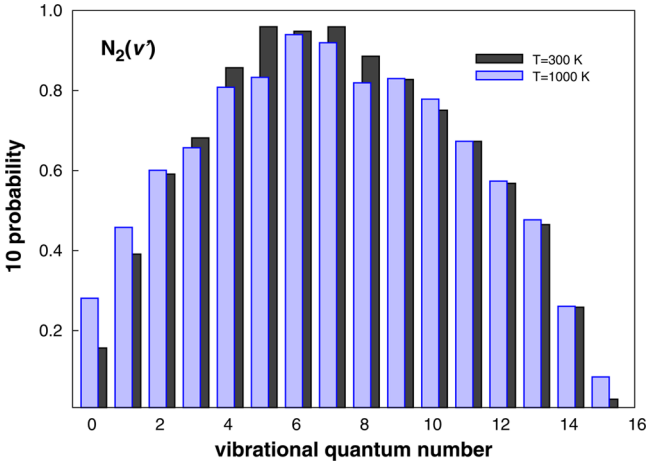

Figure 8. Total vibrational distribution for product N_2 in the N + $NO(v, j = 1)$ reaction under different temperatures: solid line, T = 300 K; dashed line, T = 1000 K.

see ref 49 for a similar pattern for the O + OH reaction. Also indicated for comparison in Figure 5 are the theoretical results by González et al.[27] Their smaller values do not show any obvious temperature-dependence, being 6 times smaller than ours.

The dependence of the state-specific cross section of reaction 2, as a function E_{tr} for the $NO(v = 0,j = 1)$ reaction, is given in Table 2 and shown in Figure 6. To model the collision energy dependence of the calculated cross sections, we have employed the form

$$\sigma(E_{tr}) = a + bE_{tr}^{n} \tag{19}$$

with optimum parameters being defined as follows: a = −79.6 Å^2, b = 150.4 Å^2(kcal mol^{-1})$^{-n}$, and n = −0.136. Note that the value of b_{max} increases with decreasing translation energy while for higher translation energies it is essentially constant or slightly increases with E_{tr}. A similar behavior has been described elsewhere for OH + O_2 reaction.[50] Thus, we expect N_2O formation to be dictated in the present case by a capture-type mechanism where long-range forces play an important role. Such a dependence of b_{max} on E_{tr} may therefore be rationalized as follows: the dominant contribution for the interaction between $N(^2D)$ and $NO(X\ ^2\Pi)$ arises from the long-range electrostatic term[51−53] involving the quadrupole moment of atomic nitrogen and the dipole moment of NO, and also the quadrupole moment of N and the quadrupole moment of NO. Since the NO stretching leads to an increase of its electric quadrupole moment, it may then be expected to yield a more attractive long-range interaction. This may explain why b_{max} increases with decreasing translation energy. Conversely, for high translation energy, long-range forces should be less

dx.doi.org/10.1021/jp408487y | J. Phys. Chem. A 2014, 118, 1277−1286

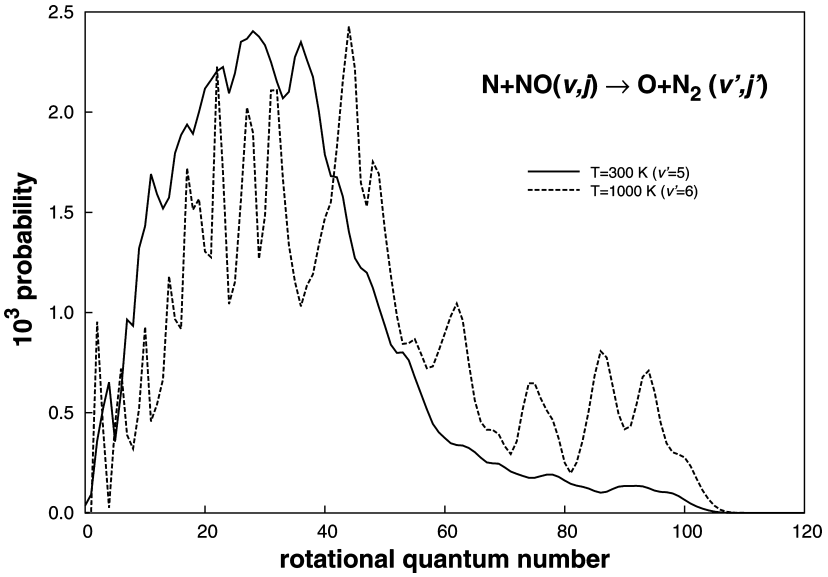

Figure 9. Comparison for the rotational distribution of the most populated N_2 vibrational state $\nu' = 5$, $\nu' = 6$ for $T = 300$ and 1000 K, respectively.

important for reaction, leading only to a small decrease in b_{max}. In summary, the cross sections of reaction 2 strongly decrease with E_{tr} in the 0.1−1 kcal mol^{-1} range, with a gradual stabilization then occurring until the cross section becomes nearly independent of E_{tr} above 5 kcal mol^{-1}.

Additional calculations of the N-exchange reaction (eq 5) have also been carried out, with the results being reported in Tables 2 and 3. The results show that the rate constant decreases with T between 5 and 200 K and then increases from 300 to 3000 K. A significant contribution of the N-exchange reaction is therefore expected at high temperatures. In turn, the cross sections of the N-exchange reaction decrease with translation energy while, for high temperatures, they become essentially constant or manifest a slight decrease with E_{tr}.

3.3. Rovibrational Product Analysis. The analysis of vibrational and rotational distribution for the newly formed N_2 on the DMBE PES has been studied by the momentum Gaussian-binning (shortly MGB) method.[54] Briefly, the probability of a rovibrational state (υ,j) is given by

$$P_{\upsilon j} = \sum_{i=1}^{N} \frac{W_{\upsilon j}^{i}}{N_r} \tag{20}$$

where $W_{\upsilon j}^{i} \sim W_{\upsilon}^{i} W_{j}^{i}$ and

$$W_{k}^{i} = \frac{1}{\rho k \sqrt{\pi}} \exp\left[-\left(\frac{\sqrt{E_k} - \sqrt{\varepsilon_k^i}}{\rho k \sqrt{\overline{E}_k}} \right)^2 \right] \tag{21}$$

where E_k is the kth diatomic energy eigenvalue, $\overline{E}_k$ is an average separation between neighboring levels, and ε_k^i is the final energy of the ith trajectory (vibrational or rotational). The separation of the internal energy is carried out using the standard procedure;[42] that is, after the end of trajectory is reached, 200 circles are used to obtain the rotational energy while vibrational energy is obtained by the difference with the internal energy. It should be noted that the MGB differs slightly from the GB,[55] as suggested by the theory. In fact, the weights should reflect a squared Gaussian dependence on the displacements from the square-root of the energy of a given contributing state to the supposedly known classical value (viewed as the centroid of the relevant quantum distribution).[54]

Figure 7 shows a contour for the state-specific probabilities as a function of the product's rovibrational level for $T = 300$ K and $T = 1000$ K. As it can be seen, the highest probability occurs for $\upsilon' = 8$ and $j' = 29$ for $T = 300$ K, whereas for $T = 1000$ K it displays a broader bimodal distribution centered at $\upsilon' = 8$ and $\upsilon' = 0$. Figure 8 compares the vibrational distributions obtained from the MGB scheme for $T = 300$ K and $T = 1000$ K. The results show only small differences, with a peak at $\upsilon' = 5$ for $T = 300$ K, while, for the larger temperature $T = 1000$ K, the peak is at $\upsilon' = 6$, as expected for an exothermic reaction. Significant differences arise, though in the corresponding vibrationally specific rotational distributions. This is illustrated in Figure 9, which corresponds to the maximum populated vibrational states, $\upsilon' = 5$ and $\upsilon' = 6$. It presents a peak at about $j' = 25$ and $j' = 41$, at $T = 300$ K and $T = 1000$ K, respectively. By checking the probability of the rotational states for each of the temperatures calculated for the title system, we have found that, at $T = 300$ K, the probability for the $j' = 0$−41 levels lies higher than that for $T = 1000$ K obtained for their corresponding υ' state. This relation is inverted when $j' > 41$ until the probability goes to 0.

4. CONCLUDING REMARKS

In spite of its importance, the title multichannel reaction has only a few theoretical studies so far due to lack of realistic PESs. Our motivation in this work has been to cover this gap and hence initiate a series of studies using a DMBE PES for the ground state of N_2O that we have recently proposed.[31] Specifically, we have carried out a QCT study of the rate constant for the $N(^2D)$ + $NO(X\ ^2\Pi)$ reaction, with the prediction that only a relatively small variation is expected over a wide temperature range (50−3000 K). We have reported cross sections as a function of the translation energy, which depicted the following behavior: the cross section increases with decreasing translation energy at low collision energies while for higher ones σ becomes essentially constant or just slightly increases with E_{tr}. Extensive comparisons with previous experimental and theoretical predictions have also been

dx.doi.org/10.1021/jp408487y | J. Phys. Chem. A 2014, 118, 1277−1286

performed, with the results showing a higher reactivity than others available in the literature. An improved agreement with the experimental results has therefore been obtained, even though there are large experimental uncertainties. Since nitrous oxide is known to be important in the chemistry of both the atmosphere[8] and combustion[7] with many reactions occurring on the potential energy surface studied in the present work (and others, some under investigation in our group), we hope that the present study may help with rationalization of the observed data.

AUTHOR INFORMATION

Corresponding Author

*E-mail: varandas@uc.pt.

Notes

The authors declare no competing financial interest.

ACKNOWLEDGMENTS

This work was financed by FEDER through Programa Operacional Factores de Competitividade-COMPETE and national funds under the auspices of Fundação para a Ciência e a Tecnologia, Portugal (Projects PTDC/QEQ-COM/3249/2012, PTDC/AAG-MAA/4657/2012, and SFRH/BD/66471/2009).

REFERENCES

(1) Ravishankara, A. R.; Daniel, J. S.; Portmann, R. W. Nitrous Oxide (N_2O): The Dominant Ozone-Depleting Substance Emitted in the 21st Century. *Science* **2009**, *326*, 123−125.

(2) Phillips, L. F.; Schiff, H. I. Mass Spectrometric Studies of Atom Reactions. 1. Reactions in the Atomic Nitrogen-Ozone System. *J. Chem. Phys.* **1962**, *36*, 1518.

(3) Husain, D.; Slater, N. K. H. Kinetic Study of Ground State Atomic Nitrogen, $N(2^4S_{3/2})$, by Time-Resolved Atomic Resonance Fluorescence. *J. Chem. Soc., Faraday Trans II* **1980**, *76*, 606−619.

(4) Cheah, C. T.; Clyne, M. A. A. Reactions Forming Electronically-excited Free Radicals Part 2. Formation of N^4S, N^2D and N^2P Atoms in the H + NF_2 Reaction, and N Atom Reactions. *J. Chem. Soc., Faraday Trans II* **1980**, *76*, 1543−1560.

(5) Gilibert, M.; Aguilar, A.; González, M.; Mota, F.; Sayós, R. Dynamics of the $N(^4S_u)$ + $NO(X\ ^2\Pi)$ → $N_2(X\ ^1\Sigma_g^+)$ + $O(^3P_g)$ Atmospheric Reaction on the $^3A''$ Ground Potential Energy Surface. I. Analytical Potential Energy Surface and Preliminary Quasiclassical Trajectory Calculations. *J. Chem. Phys.* **1992**, *97*, 5542−5553.

(6) Herron, J. T. Evaluated Chemical Kinetics Data for Reactions of N^2D, N^2P, and $N_2(A^3\Sigma_u^+)$ in the Gas Phase. *J. Phys. Chem. Ref. Data* **1999**, *28*, 1453−1483.

(7) Dean, A. M.; Bozzelli, J. W. In *Gas-Phase Combustion Chemistry*; Gardiner, J. W. C., Ed.; Springer: New York, 2000; pp 125−341.

(8) Wayne, R. P. *Chemistry of Atmospheres*, 3rd ed.; Oxford University Press: 2000.

(9) Gamallo, P.; Martínez, R.; Sayós, R.; González, M. Quasiclassical Dynamics and Kinetics of the N + NO → N_2 + O,NO + N Atmospheric Reactions. *J. Chem. Phys.* **2010**, *132*, 144304.

(10) Hopper, D. G. *Ab initio* Multiple Root Optimization MCSCF Study of the $C_{\infty v}/C_s$ Excitation Spectra and Potential Energy Surfaces of N_2O. *J. Chem. Phys.* **1984**, *80*, 4290−4316.

(11) Donovan, R. J.; Husain, D. Recent Advances in the Chemistry of Electronically Excited Atoms. *Chem. Rev.* **1970**, *70*, 489−516.

(12) Brouard, M.; Duxon, S. P.; Enriquez, P. A.; Simons, J. P. The Stereochemistry of the $O(^1D)$ + N_2O → NO + NO Reaction via Velocity-aligned Photofragment Dynamics. *J. Chem. Phys.* **1992**, *797*, 7414−7422.

(13) Black, G.; Slanger, T. G.; John, G. A. S.; Young, R. A. Vacuum-Ultraviolet Photolysis of N_2O. IV. Deactivation of $N(^2D)$. *J. Chem. Phys.* **1969**, *51*, 116−121.

(14) Lin, C.; Kaufman, F. Reactions of Metastable Nitrogen Atoms. *J. Chem. Phys.* **1971**, *55*, 3760−3770.

(15) Husain, D.; Kirsch, L. J.; Wiesenfeld, J. R. Collisional Quenching of Electronically Excited Nitrogen Atoms, $N(2^2D_J,2^2P_J)$ by Time-resolved Atomic Absorption Spectroscopy. *Faraday Discuss. Chem. Soc.* **1972**, *53*, 201.

(16) Husain, D.; Mitra, S. K.; Young, A. N. Kinetic Study of Electronically Excited Nitrogen Atoms, $N(2^2D_J,2^2P_J)$, by Attenuation of Atomic Resonance Radiation in the Vacuum Ultra-violet. *J. Chem. Soc., Faraday Trans. 2* **1974**, *70*, 1721−1731.

(17) Sugawara, K.; Ishikawa, Y.; Sato, S. The Rate Constants of the Reactions of the Metastable Nitrogen Atoms, ^2D and ^2P, and the Reactions of $N(^4S)$ + NO → N_2 + $O(^3P)$ and $O(^3P)$ + NO + M → NO_2 + M. *Bull. Chem. Soc. Jpn.* **1980**, *53*, 3159−3164.

(18) Umemoto, H.; Hachiya, N.; Matsunaga, E.; Suda, A.; Kawasaki, M. Rate Constants for the Deactivation of $N(2^2D)$ by Simple Hydride and Deuteride Molecules. *Chem. Phys. Lett.* **1998**, *296*, 203−207.

(19) Brown, A.; Jimeno, P.; Balint-Kurti, G. G. Photodissociation of N_2O. I. *Ab Initio* Potential Energy Surfaces for the Low-Lying Electronic States $\tilde{X}^1A'$, $2\ ^1A'$, and $1\ ^1A''$. *J. Phys. Chem. A* **1999**, *103*, 11089−11095.

(20) Johnson, M. S.; Billing, G. D.; Gruodis, A.; Janssen, M. H. M. Photolysis of Nitrous Oxide Isotopomers Studied by Time-Dependent Hermite Propagation. *J. Phys. Chem. A* **2001**, *105*, 8672−8680.

(21) Daud, M. N.; Balint-Kurti, G. G.; Brown, A. *Ab initio* Potential Energy Surfaces, Total Absorption Cross Sections, and Product Quantum State Distributions for the Low-lying Electronic States of N_2O. *J. Chem. Phys.* **2005**, *122*, 054305.

(22) Nanbu, S.; Johnson, M. S. Analysis of the Ultraviolet Absorption Cross Sections of Six Isotopically Substituted Nitrous Oxide Species Using 3D Wave Packet Propagation. *J. Phys. Chem. A* **2004**, *108*, 8905−8913.

(23) Schinke, R. Photodissociation of N_2O: Potential Energy Surfaces and Absorption Spectrum. *J. Chem. Phys.* **2011**, *134*, 064313.

(24) Schinke, R.; Schmidt, J. A.; Johnson, M. S. Photodissociation of N_2O: Triplet States and Triplet Channel. *J. Chem. Phys.* **2011**, *135*, 194303.

(25) Schmidt, J. A.; Johnson, M. S.; Schinke, R. Isotope Effects in N_2O Photolysis From First Principles. *Atmos. Chem. Phys.* **2011**, *11*, 8965−8975.

(26) Schmidt, J. A.; Johnson, M. S.; Lorenz, U.; McBane, G. C.; Schinke, R. Photodissociation of N_2O: Energy Partitioning. *J. Chem. Phys.* **2011**, *135*, 024311.

(27) González, M.; Valero, R.; Sayós, R. *Ab initio* and Quasiclassical Trajectory Study of the $N(^2D)$ + $NO(X\ ^2\Pi)$ → $O(^1D)$ + $N_2(X\ ^1S_g^+)$ Reaction on the Lowest $^1A'$ Potential Energy Surface. *J. Chem. Phys.* **2000**, *113*, 10983−10998.

(28) Varandas, A. J. C. Modeling and Interpolation of Global Multi-sheeted Potential Energy Surface. In *Conical Intersections: Electronic Structure, Spectroscopy and Dynamics*; Domcke, W., Yarkony, D. R., Köppel, H., Eds.; Adv. Series Phys. Chem.; World Scientific Publishing: 2004; Vol. *15*; Chapter 5, pp 205−270.

(29) Varandas, A. J. C. Intermolecular and Intramolecular Potentials: Topographical Aspects, Calculation, and Functional Representation via a DMBE Expansion Method. *Adv. Chem. Phys.* **1988**, *74*, 255−338.

(30) Varandas, A. J. C. Multivalued Potential Energy Surfaces for Dynamics Calculations. In *Lecture Notes in Chemistry*; Laganá, A., Riganelli, A., Eds.; Springer: Berlin, 2000; Vol. *75*; pp 33−56.

(31) Li, J.; Varandas, A. J. C. Accurate Ab-initio-based Single-sheeted DMBE Potential-Energy Surface for Ground-State N_2O. *J. Phys. Chem. A* **2012**, *116*, 4646−4656.

(32) Werner, H. J.; Knowles, P. J. An Efficient Internally Contracted Multiconfiguration-reference Configuration Interaction Method. *J. Chem. Phys.* **1988**, *89*, 5803−5814.

(33) Knowles, P. J.; Werner, H.-J. An Efficient Method for the Evaluation of Coupling Coefficients in Configuration Interaction Calculations. *Chem. Phys. Lett.* **1988**, *145*, 514−522.

(34) Kendall, R. A.; Dunning, T. H., Jr.; Harrison, R. J. Electron Affinities of the First-row Atoms Revisited. Systematic Basis Sets and Wave Functions. *J. Chem. Phys.* **1992**, *96*, 6796−6806.
(35) Dunning, T. H., Jr. Gaussian Basis Sets for Use in Correlated Molecular Calculations. I. The Atoms Boron Through Neon and Hydrogen. *J. Chem. Phys.* **1989**, *90*, 1007−1024.
(36) Murrell, J. N.; Carter, S.; Farantos, S. C.; Huxley, P.; Varandas, A. J. C. *Molecular Potential Energy Surfaces*; Wiley: New York, 1984.
(37) Krishnan, R.; Binkley, J. S.; Pople, J. A. Self-consistent Molecular Orbital Methods. XX. A Basis Set for Correlated Wave Functions. *J. Chem. Phys.* **1980**, *72*, 650−654.
(38) Frish, M. J.; Pople, J. A.; Binkley, J. S. Self-consistent Molecular Orbital Methods 25. Supplementary Functions for Gaussian Basis Sets. *J. Chem. Phys.* **1984**, *80*, 3265−3269.
(39) Varandas, A. J. C. A Semiempirical Method for Correcting Configuration Interaction Potential Energy Surfaces. *J. Chem. Phys.* **1989**, *90*, 4379−4391.
(40) Varandas, A. J. C. A Useful Triangular Plot of Triatomic Potential Energy Surfaces. *Chem. Phys. Lett.* **1987**, *138*, 455−461.
(41) Varandas, A. J. C. General discussion. *Faraday Discuss. Chem. Soc.* **1987**, *84*, 351−357.
(42) Peslherbe, G. H.; Wang, H.; Hase, W. L. Monte Carlo Sampling for Classical Trajectory Simulations. *Adv. Chem. Phys.* **1999**, *105*, 171−201.
(43) Hase, W. L.; Duchovic, R. J.; Hu, X.; Komornicki, A.; Lim, K. F.; Lu, D.; Peslherbe, G. H.; Swamy, K. N.; Linde, S. R. V.; Varandas, A. J. C.; et al. VENUS96: A General Chemical Dynamics Computer Program. *QCPE Bull.* **1996**, *16*, 43.
(44) Varandas, A. J. C.; Brandão, J.; Pastrana, M. R. Quasiclassical Trajectory Calculations of the Thermal Rate Coefficients for the Reactions H(D) + O_2 → OH(D) + O and O + OH(D) → O_2 + H(D) as a Function of Temperature. *J. Chem. Phys.* **1992**, *96*, 5137−5150.
(45) Caridade, P. J. S. B.; Varandas, A. J. C. Dynamics Study of the N(^4S) + O_2 Reaction and Its Reverse. *J. Phys. Chem. A* **2004**, *108*, 3556−3564.
(46) LeRoy, R. L.*LEVEL 7.5, A Computer Program for Solving the Radial Schrödinger Equation for Bound and Quasi-bound Levels*; University of Waterloo Chemical Physics Research Report; 2002; http://leroy.waterloo.ca/
(47) Fell, C.; Steinfeld, J. I.; Miller, S. Quenching of N(^2D) by O(^3P). *J. Chem. Phys.* **1990**, *92*, 4768−4778.
(48) LeRoy, R. L. *J. Phys. Chem.* **1969**, *73*, 4338−4344.
(49) Varandas, A. J. C. Accurate Combined-hyperbolic-inverse-power-representation of *Ab initio* Potential Energy Surface for the Hydroperoxyl Radical and Dynamics Study of O + OH Reaction. *J. Chem. Phys.* **2013**, *138*, 134117.
(50) Garrido, J. D.; Caridade, P. J. S. B.; Varandas, A. J. C. Dynamics Study of the HO(v' = 0) + O_2(v'') Branching Atmospheric Reaction. 1. Formation of Hydroperoxyl Radical. *J. Phys. Chem.* **1999**, *103*, 4815−4822.
(51) Martínez-Núñez, E.; Varandas, A. J. C. Single-Valued DMBE Potential Energy Surface for HSO: A Distributed *n*−Body Polynomial Approach. *J. Phys. Chem. A* **2001**, *105*, 5923−5932.
(52) Rodrigues, S. P. J.; Sabn, J. A.; Varandas, A. J. C. Single-Valued Double Many-Body Expansion Potential Energy Surface of Ground-State SO_2. *J. Phys. Chem. A* **2002**, *106*, 556−562.
(53) Varandas, A. J. C.; Rodrigues, S. P. J. New Double Many-body Expansion Potential Energy Surface for Ground-state HCN from a Multiproperty Fit to *Ab Initio* Energies and Rovibrational Data. *J. Phys. Chem. A* **2006**, *110*, 485−493.
(54) Varandas, A. J. C. Trajectory Binning Scheme and Non-active Treatment of Zero-point Energy Leakage in Quasi-classical Dynamics. *Chem. Phys. Lett.* **2007**, *439*, 386−392.
(55) Bonnet, L.; Rayez, J. Quasiclassical Trajectory Method for Molecular Scattering Processes: Necessity of a Weighted Binning Approach. *Chem. Phys. Lett.* **1997**, *277*, 183.